Magazine of Civil Engineering

ISSN 2712-8172

journal homepage: http://engstroy.spbstu.ru/

Research article

UDC 624.12

DOI: 10.34910/MCE.139.5

Flow turbulence conditions and sensitivity of bucket-type spillway geometry parameters in energy dissipation

S. Mohammadalizadeh[1] ✉ , ***A. Yasaei***[2], ***A. Mardookhpour***[2]

[1] *Islamic Azad University, Lahijan Branch, Lahijan, Iran*

[2] *Islamic Azad University, Lahijan Branch, Department of Civil Engineering, Lahijan, Iran*

✉ *saeidmhmdalizadeh74@gmail.com*

Keywords: bucket spillway, energy dissipation, throw length, throw height, throw angle, RNG turbulence model, (k-ε) turbulence model, Flow-3D software

Abstract. Energy dissipation downstream of dams is considered one of the important issues in these structures. Various structures have been employed to perform this function. Among them, bucket-type spillways are of great importance, where the outflow jet from these structures faces complex issues, including jet diffusion and downstream erosion. With the hardware and software advancement of numerical simulation systems, the evaluation of this phenomenon is possible at a lower cost compared to laboratory conditions. In this research, using FLOW-3D software and the RNG turbulence model, the effects of various geometric and hydraulic parameters related to the bucket-type spillway on the outflow jet have been investigated. The results of the RNG turbulence model show better agreement with laboratory results compared to the (k-ε) turbulence model. The relative error in energy reduction between laboratory results and numerical model results is less than 5%, and the error related to maximum jump length is less than 7%. The changes in spillway geometry include changes in the spillway angle from 52° to 32° and changes in the spillway arc radius from 12-19 cm.

Citation: Mohammadalizadeh, S., Yasaei, A., Mardookhpour, A. Flow Turbulence conditions and sensitivity of bucket-type spillway geometry parameters in energy dissipation. Magazine of Civil Engineering. 2026. 18(7). Article no. 13905. DOI: 10.34910/MCE.139.5

1. Introduction

Energy dissipation downstream of high dams constitutes a serious problem. When high flow velocities exist, stilling basins present problems of cavitation and erosion, so they are used as ski jump spillways. Therefore, this energy dissipation system is widely used and seemingly is the only structure that is both technically and hydraulically suitable and safe for excess flow energy control. Although numerous ski-jump spillways have been constructed to date, most have been designed based on physical models and regional studies, and no standard design guidelines exist in this field. In recent years, numerical methods, including three-dimensional Computational Fluid Dynamics (CFD), have rapidly developed due to advances in computer technology and numerical methods. CFD models are more flexible than physical models and require less time and cost; furthermore, due to the use of actual prototype dimensions in these models, scale effects are eliminated. CFD analyses are extensively used in fluid mechanics applications such as multiphase flows and free surface flows. When CFD analysis results, numerical validations, and prototype observations demonstrate appropriate correlation with one another, the results of numerical modeling may be utilized. In this research, through numerical investigation of flow over ogee spillways with flat ski-jump buckets using FLOW 3D software, models with different geometries in ski-jump buckets have

been examined, and various parameters, including Froude numbers, different discharge rates, geometries with different launch angles, and different arc radii have been investigated.

With the increasing trend in constructing high dams and rising dam safety standards, hydraulic engineers have shown a growing interest in designing reliable and economical energy dissipation systems at the terminals of main flood discharge channels in high dams. Energy dissipation structures are facilities placed at the end of dam spillways to dissipate water flow energy. Among various types of energy dissipation structures, three types (stilling basins with hydraulic jump, roller dissipators, and bucket-type dissipators) are widely used in dams [1].

The use of free-falling jets in bucket-type spillways (along with associated plunge pools), given suitable geological and topographical conditions, offers significant economic and safety advantages compared to other types of energy dissipation structures. In high dams, bucket spillways, utilizing the high velocity of inflow to the bucket, can deflect the flood discharge from the spillway as a free-falling jet in such a way that it falls at a safe distance from the spillway and dam into the plunge pool or river bed. The optimal design of a bucket-type spillway, in addition to proper positioning, geometric shape, and appropriate dimensions, requires extensive study of scour and analysis of excess flow energy dissipation efficiency. This necessitates calculation and analysis of flow variables and geometric parameters related to the spillway, as improper design without proper analysis of these parameters could damage the structure and ultimately lead to irreparable damage to the chute the dam itself and cause adverse effects on the stilling basin and downstream areas [1].

Olsen et al. (1998) examined the performance of FLOW-3D simulation in analyzing pressure values and discharge over an ogee spillway. The results obtained from numerical simulation showed acceptable agreement when compared with physical simulation values [2]. Meilan et al. (2000) conducted studies on bed erosion caused by vertical and oblique water jet impact in submerged conditions. The results showed that at low velocities, scour volume changes with jet velocity, such that increasing the jet angle also increases scour volume. However, at high velocities, the effect of jet angle is not significant [3].

Savage and Johnson (2001) studied a standard ogee spillway through FLOW-3D software. The numerical analysis results matched well with experimental findings according to the study [4]. Ho et al. (2003) utilized computational fluid dynamics to model spillway behaviors across two-dimensional and three-dimensional domains at different water height levels which yielded results that matched field data measurements [5]. Free-flow spillway modeling with an S-shaped plan was performed by Sarker and Rhodes (2002) using FLUENT software. The standard turbulence model accompanied the VOF multiphase flow model for performing simulations. The RNG model demonstrated the most accurate correlation between numerical and physical results regarding average velocity according to the research in [6].

The research conducted by Weilin et al. (2004) investigated how jet velocity influences the main dimensions of flat jet scour holes. The authors established that higher velocity at all tailwater depths along with various bed particle types, results in deeper and longer scour holes. The length and depth of scour holes decrease when tailwater depth increases with constant velocity and particle size [7]. Heller et al. (2005) conducted experiments on circular bucket spillway outflow to study jet pressure parameters together with jet trajectory and downstream wave formation. The experimental results indicated that both Froude numbers and surface curvature and surface angle proved to be significant factors in this study. The use of these parameters proved essential for ski jump design because they directly affected the overall functionality [8].

Pagliara et al. (2006) conducted approximately 60 experiments studying the effect of upstream flow velocity at jet impact location in the tailwater on scour hole dimensions. They presented an equation for scour depth as a function of upstream Froude number. They concluded that with increasing the Froude number, suspended sediments in the scour hole are transported downstream, the scour hole deepens, and the downstream mound gradually decreases due to erosion [9]. Dargahi (2006) performed a three-dimensional numerical simulation of an ogee spillway in his study, comparing the water surface profile and discharge coefficient with experimental results, which fell within an accuracy range of 5.1 to 9.2% [10].

Steiner et al. (2008) conducted research on pressure distribution in ski jump energy dissipators with triangular buckets by using experimental models. The researchers evaluated how the spillway's hydraulic performance worked in this particular configuration by studying pressure distribution on the bucket along with angle effects on downstream motion. The circular bucket design proved to be the most optimal among all tested shapes, according to their findings [11]. Kavianpour Esfahani et al. (2011) performed experimental research that studied the impact of discharge rates and tailwater depths on bucket-type spillway jet flow scour patterns. The hydraulic model study conducted at the Azad Dam flood discharge system revealed that variations in discharge rate and tailwater depth substantially affect the maximum scour depth [12].

Arefpour et al. (2012) studied hydrodynamic pressure distribution and instantaneous pressure fluctuations along a bucket-type spillway using the Balaroud Dam experimental model, testing six different

return period discharges. Results from measuring minimum and maximum dynamic pressure fluctuations indicated that these fluctuations do not have a destructive effect on the structure [13].

Mousavi Jahromi and Omidvarinia (2012) studied ski jumps in triangular-type spillways with geometry different from bucket-type spillways. The researchers conducted a hydraulic performance study that compared triangular bucket spillways against circular bucket spillways with specific emphasis on outflow trajectory effects. A physical prototype of the ogee spillway underwent testing by changing both the discharge rates and the flow angles. An increase in flip bucket angle resulted in thinner outflow jet thickness while changing Froude numbers between 41.6 and 44.4, which extended the travel length [14].

Askari and Ghomeshi (2013) demonstrated through experimental modeling of an ogee spillway with a bucket-type flip bucket, using various discharges and angles, that different angles result in varying energy dissipation rates. Energy loss percentage increases with higher Froude numbers [15]. Nikpour et al. (2014) analyzed flow over an ogee spillway using the k-ε turbulence model, employing finite element and finite volume methods in two dimensions with FLUENT software. The model accuracy in determining water surface profile and flow velocity assessment was conducted by comparing simulation results against measured values. The numerical models showed effective performance in determining free water surface profiles according to the study results [16].

Eshrati et al. (2015) created a physical model of a free ogee-type spillway with a curved plan to conduct tests. The researchers analyzed spillway efficiency results that compared normal and submerged conditions at equal discharges. The researchers determined that axial curve spillways produce a 21% increase in discharge coefficient when compared to straight-crested spillways at equivalent hydraulic and geometric conditions [17].

Kakeshpour et al. (2016) utilized FLOW-3D software for numerical modeling derived from the Balaroud Dam spillway physical model research. The analysts utilized the VOF method with the RNG turbulence model to evaluate flip bucket designs that used circular and triangular shapes. Numerical and experimental models produced results that differed by 15%. The researchers analyzed how the Froude number related to the cavitation number within the chute end zone and flip bucket space while identifying that maximum erosion potential emerges at a specific critical point that might not match the peak Froude number [18].

Fazlollahnejad et al. (2016) modeled and studied hydraulic flow characteristics over a converging chute and bucket-type spillway with a negative slope at Gotvand Neka Dam using FLOW-3D software. Comparing results from modified spillway geometry to the original model, they found that changing the circular arc radius did not significantly affect hydraulic characteristics, with only a 5m increase in throw length observed with increased radius [19].

Zhenwei et al. (2012) modeled spillway flow using the VOF model in FLUENT computational fluid dynamics software. The modeling results agreed with the experimental model regarding pressure, free surface fluid level, and flow velocity along the spillway [20]. Sharifi and Rostami Ravori (2013) conducted experiments and modeling on various geometries, including flat chute with a 40° flip bucket angle and a compound chute with two different angle combinations (20 and 40°) and (40 and 80°). They modeled results using FLOW-3D and compared depth and energy curves, finding that compound flip buckets with lower angles demonstrated greater energy dissipation capability [21].

Fadaei Kermani and Barani (2014) conducted a numerical analysis of bucket-type flip buckets through the implementation of the RNG turbulence model to study pressure and velocity variations. The numerical calculations performed for piezometric pressure and velocity near the spillway showed maximum differences between experimental and calculated results of 47.5% for average velocity values and 79.7% for pressure values [22].

Parsaie et al. (2016) studied numerical modeling of cavitation phenomena on Balaroud Dam spillway bucket surfaces. This research compared numerical modeling performance with a physical model built for this purpose. During numerical modeling, they found the RNG turbulence model suitable for cavitation modeling. Physical modeling showed a minimum cavitation index of around 0.85, while FLOW-3D results yielded approximately 0.1665, with the main difference between numerical and physical modeling related to velocity. Numerical simulation results indicated that cavitation does not occur along the spillway based on a cavitation index of 0.25 [23].

Regarding the necessity and importance of this research, it can be stated that given the significance of energy dissipation in high dams, their spillways with ski-jump buckets are of particular importance. Energy dissipation in such spillways is related to various hydraulic and geometric factors of the structure, requiring appropriate investigation to achieve the highest dissipation efficiency. To date, comprehensive efforts have not been made to obtain the complete set of parameters used in designing such structures with ski-jump buckets. Obtaining these optimal geometric and hydraulic conditions for the structure and its

outlet jet is of paramount importance and must be investigated, considering its impact on downstream scour and erosion. Geometric and hydraulic parameters are examined and modeled with software so that conditions that give maximum dissipation with minimal downstream effects can be approached.

The objective of this research is to investigate flow turbulence conditions and the sensitivity of ski-jump bucket geometric parameters and flow hydraulics relative to energy dissipation. The general objectives are itemized as follows:

1. Evaluation of turbulence models and selection of appropriate models for use in ski-jump spillways
2. Investigation of geometric parameters related to ski-jump buckets
3. Investigation of hydraulic parameters related to flow
4. Assessment of the sensitivity of bucket geometric parameters and flow hydraulics relative to energy dissipation

2. Materials and Methods

The section begins with presentations of continuity and momentum equations before explaining turbulence models active in software programs including the K-ε model. The research software FLOW-3D receives further description in this section.

2.1. Computational Fluid Dynamics

Theoretical methods begin with observing physical phenomena, expressing the relevant differential equations, and then addressing the algebraic equations governing the problem. The challenge is that, unlike phenomena for which appropriate mathematical models have been developed (such as laminar flow), there are phenomena for which suitable mathematical models have not yet been found (such as two-phase flows). Numerical methods function as the third approach for solving fluid flow problems because of their known limitations. Three categories make up the entire field of fluid dynamics according to [24].

- Experimental Fluid Dynamics
- Theoretical Fluid Dynamics
- Computational Fluid Dynamics

The CFD method serves as a fluid mechanics branch dedicated to analyzing fluid flow problems through numerical analysis paired with numerical algorithms. Computers operate simulations which model the interaction between liquids and gases with boundary condition surfaces. This fluid mechanics branch connects classical mechanics with the modern computational capabilities of computer science during the new millennium [24].

The CFD method is the structure of numerical programs, and numerical algorithms include the following steps [24]:

- Integration of fluid flow governing equations over all control volumes related to the solution field
- Discretization, including substitution of finite difference approximations for terms within the integral equation, which represents flow processes such as convection, diffusion, and sources. This process converts integral equations into a system of algebraic equations
- Solving algebraic equations using an iterative method. CFD in fluid system design has several unique advantages over experimental methods
- Substantial reduction in time and cost of new designs
- Ability to study systems where experiments are difficult or impossible
- Ability to study systems under random conditions and beyond their normal limits

Discretization methods for differential equations in computational dynamics [24]:

- Finite Element Method
- Finite Volume Method
- Finite Difference Method
- Spectral Methods

The finite volume method provides superior application in modeling incompressible flow systems. Computational fluid dynamics commercial software companies have primarily developed their products through this method [24].

2.2. Flow Equations

Fluid dynamics function through flow equations, which result from three fundamental physical conservation laws for mass, momentum, and energy. The governing equations of fluid flow represent mathematical expressions of physical conservation laws according to [24].

- The principle of mass conservation leads to flow continuity equations
- The principle of momentum conservation leads to momentum equations
- The principle of energy conservation leads to flow energy equations

2.3. Continuity Equation

Mass conservation of a small fluid element proves that the total mass flux into the element equals the element's mass growth rate through the relation below:

$$\frac{\partial \rho}{\partial t}+\frac{\partial(\rho u)}{\partial x}+\frac{\partial(\rho v)}{\partial y}+\frac{\partial(\rho \omega)}{\partial z}=0. \tag{1}$$

The relationship for incompressible fluids reduces to this form:

$$\mathrm{div}U=\frac{\partial u}{\partial x}+\frac{\partial v}{\partial y}+\frac{\partial \omega}{\partial z}=0. \tag{2}$$

The equations include spatial coordinates $x,\ y,\ z$ along with velocity components $u,\ v,\ w$ that operate in the directions of $x,\ y,\ z$. The fluid velocity takes vector form through U and combines with fluid density which is represented by ρ [24].

2.4. Momentum Equation

When applying the principle of conservation of momentum to a designated fluid element, you find that acting forces balance the rate at which fluid momentum increases within that element. The fluid particle experiences two types of forces which include pressure forces acting on the surface and gravitational forces acting as body forces. This principle has a mathematical expression that works in different directions (x, y and z) as follows [24]:

$$\begin{cases} \rho\dfrac{Du}{Dt}=\dfrac{\partial(-P+\tau_{xx})}{\partial x}+\dfrac{\partial \tau_{xy}}{\partial y}+\dfrac{\partial \tau_{zx}}{\partial z}+S_{MX} \\ \rho\dfrac{Dv}{Dt}=\dfrac{\partial \tau_{xy}}{\partial x}+\dfrac{\partial(-P+\tau_{yy})}{\partial y}+\dfrac{\partial \tau_{zy}}{\partial z}+S_{MY} \\ \rho\dfrac{Dw}{Dt}=\dfrac{\partial \tau_{xz}}{\partial x}+\dfrac{\partial \tau_{yz}}{\partial y}+\dfrac{\partial(-P+\tau_{zz})}{\partial z}+S_{MZ} \end{cases}. \tag{3}$$

In fact, the above body forces are:

$$S_{MX}=S_{MY}=0; \tag{4}$$

$$S_{MZ}=-\rho g. \tag{5}$$

In a Newtonian fluid, viscous stresses are proportional to strain rates. The three-dimensional form of Newton's viscosity for compressible flows contains two constants: dynamic viscosity (μ) and secondary viscosity (λ). Considering these, the surface stresses will be:

$$\begin{cases} \tau_{xx} = 2\mu\dfrac{\partial u}{\partial x} + \lambda \mathrm{div}U \rightarrow \tau_{yx} = \tau_{xy} = \mu\left(\dfrac{\partial u}{\partial y} + \dfrac{\partial v}{\partial x}\right) \\ \tau_{yy} = 2\mu\dfrac{\partial v}{\partial y} + \lambda \mathrm{div}U \rightarrow \tau_{xz} = \tau_{zx} = \mu\left(\dfrac{\partial u}{\partial z} + \dfrac{\partial w}{\partial x}\right) \\ \tau_{zz} = 2\mu\dfrac{\partial w}{\partial z} + \lambda \mathrm{div}U \rightarrow \tau_{zy} = \tau_{yz} = \mu\left(\dfrac{\partial v}{\partial z} + \dfrac{\partial w}{\partial y}\right) \end{cases}. \quad (6)$$

Given that liquids are incompressible and have no volumetric deformation (ε = 0), and according to the continuity relation $\mathrm{div}U$ = 0, substituting the above relations into equations (3) and performing necessary simplifications yields [25]:

$$\begin{cases} \rho\dfrac{Du}{Dt} = -\dfrac{\partial p}{\partial x} + \mathrm{div}\left(\mu \mathrm{grad}u\right) + S_{MX} \\ \rho\dfrac{Dv}{Dt} = -\dfrac{\partial p}{\partial y} + \mathrm{div}\left(\mu \mathrm{grad}v\right) + S_{MY} \\ \rho\dfrac{Dw}{Dt} = -\dfrac{\partial p}{\partial z} + \mathrm{div}\left(\mu \mathrm{grad}w\right) + S_{MZ} \end{cases}. \quad (7)$$

The following relations represent fluid mechanics equations where x, y, z denote spatial directions while u, v, w represent their velocity portions and U indicates velocity vector and ρ stands for fluid density with μ representing fluid dynamic viscosity and p indicating fluid pressure at any point and s representing the source term. The Navier-Stokes equations represent these relations [24].

The governing equations require turbulence models to determine the connection between Reynolds stresses and mean flow velocity components.

2.5. Turbulent Flows

Turbulence occurs frequently in engineering problems as well as hydraulic engineering structures. Turbulence presents diverse applications that make its study a complex multifaceted field. The flow remains smooth when the Reynolds number stays below the critical limit because different fluid layers glide past one another while steady flow occurs when boundary conditions remain constant with time. The laminar flow area exists within this region. The flow behavior alters because conditions change when the Reynolds number exceeds its critical value. A high wall shear rate triggers an instability in laminar flow to cause increased momentum transfer. The establishment of turbulent points at local regions leads to flow turbulence which generates random flow patterns. The turbulence grows into a system that no longer depends on either initial or random fluctuations or irregularities. Turbulent flow exists in this region as per [25].

Various turbulent flow analysis methods are as follows [25]:

- Experimental methods
- Direct solutions of the governing dynamic equations of turbulent flow fields
- Dimensional analysis methods
- Statistical equation simplification methods

The experimental method primarily relies on constructing laboratory models. In dimensional analysis, equations are compared, and terms of lower order are neglected. Given the random and stochastic nature of turbulent flow, turbulent flow field quantities can be decomposed into two components: a permanent mean value and a fluctuating value. When applied to governing equations and time-averaged, this decomposition introduces new unknowns into the governing equations. The random and irregular motion of fluid masses in turbulent flows can also generate another type of stress; consequently, the additional terms in the equations have become known as apparent stresses or Reynolds stresses. Considering the above factors, statistical methods for equation simplification are most commonly employed in the study and analysis of turbulent flows [25].

2.6. Turbulent Flow Equations

The computational method used for solving diverse flow problems through the closure of the continuity equations and Reynolds equations together with scalar transport equations defines a turbulence model. One needs to use simplified equations representing complicated turbulent behavior to determine Reynolds stresses for time-averaged equations [26].

In 1885, Reynolds decomposed a field quantity into two components: one related to the mean flow and another related to its fluctuations [26].

$$\varphi = \overline{\varphi} + \varphi'. \tag{8}$$

The pressure and velocity components in turbulent flow take the following form:

$$V = \overline{V} + \hat{V}; \tag{9}$$

$$P = \overline{P} + P. \tag{10}$$

The substitution of relationships (9) and (10) followed by time average calculation leads to mean turbulent flow equations for continuity and momentum. The instantaneous continuity equation is:

$$\frac{\partial \rho}{\partial t} + \operatorname{div}\left(\rho V\right) = 0. \tag{11}$$

The time average of this expression results in:

$$\frac{\partial \rho}{\partial t} + \operatorname{div}\left(\rho V\right) = 0. \tag{12}$$

The time-averaged momentum equation follows a similar procedure in all directions x, y and z and yields:

$$\begin{cases} \dfrac{\partial u}{\partial t} + \operatorname{div}\left(u\overline{V}\right) = -\dfrac{1}{\rho}\dfrac{\partial P}{\partial x} + V\operatorname{div}\left(\operatorname{grad} u\right) + \left[\dfrac{-\partial\overline{u^2}}{\partial x} - \dfrac{-\partial\overline{\dot{u}\dot{v}}}{\partial y} - \dfrac{-\partial\overline{\dot{u}\dot{w}}}{\partial z}\right] \\ \dfrac{\partial v}{\partial t} + \operatorname{div}\left(v\overline{V}\right) = -\dfrac{1}{\rho}\dfrac{\partial P}{\partial y} + V\operatorname{div}\left(\operatorname{grad} v\right) + \left[\dfrac{-\partial\overline{\dot{u}\dot{u}}}{\partial x} - \dfrac{-\partial\overline{v^2}}{\partial y} - \dfrac{-\partial\overline{\dot{v}\dot{w}}}{\partial z}\right] \\ \dfrac{\partial w}{\partial t} + \operatorname{div}\left(w\overline{V}\right) = -\dfrac{1}{\rho}\dfrac{\partial P}{\partial z} + V\operatorname{div}\left(\operatorname{grad} w\right) + \left[\dfrac{-\partial\overline{\dot{u}\dot{w}}}{\partial x} - \dfrac{-\partial\overline{\dot{w}\dot{v}}}{\partial y} - \dfrac{-\partial\overline{w^2}}{\partial z}\right] \end{cases}. \tag{13}$$

The random and irregular motion of molecules causes molecular viscosity and stress. Similarly, the random and irregular motion of fluid masses in turbulent flows can generate another type of stress. Consequently, the additional terms in equations (13) are known as apparent stresses or Reynolds stresses. Due to their significant magnitude relative to molecular viscosity stresses throughout most of the flow domain, apparent stresses are of paramount importance and constitute the primary factor distinguishing between mean quantity behavior in turbulent versus laminar flow. The additional stresses appearing in the above expressions, termed Reynolds stresses, are [26]:

$$\begin{cases} \tau_{xx} = -\rho\overline{u^2} \quad \tau_{yy} = -\rho\overline{v^2} \quad \tau_{zz} = -\rho\overline{\dot{w}^2} \\ \tau_{xy} = \tau_{yx} = -\rho\overline{u'v} \quad \tau_{yz} = \tau_{zy} = -\rho\overline{\dot{v}w} \quad \tau_{xz} = \tau_{zx} = -\rho\overline{u'w} \end{cases}. \tag{14}$$

2.7. Various Turbulence Model Types

The classification of Turbulent models depends on their method of implementation in the transport equation. A single transport equation approach applies to velocity scale V for fluctuating velocity and another approach uses length scale L. More complex models also exist.

Turbulence transport model classifications rely on the methods used to determine eddy viscosity, although it may be identified as a characteristic of velocity and length. Different models fitting this context include those listed below in [26].

2.8. Zero-Equation Models (Algebraic)

Differential Models

One-equation Models

Two-equation Models

Multi-equation Models

2.9. Zero-Equation or Algebraic Model

Prandtl's mixing length theory (1925) forms the basis of the algebraic models. This is his theory through which he proposed that the turbulent viscosity is proportional to fluid density, a characteristic velocity, and a characteristic length. This model has a significant limitation in its predetermined distribution of l-meter near the wall, resulting in a large difference between the experimental results and the theoretical results. If a distribution of l-meter of width is indeed reasonably accurate, these models produce satisfactory results for velocity and shear stress (but not mean velocity or mean shear stress). The mixing length model is simple, and it is economical because the solution of differential equations is not required. Yet experimental data is very flow-dependent, and the mixing length model could no longer be used for the turbulent transport (convection and conduction (diffusion)) processes. Since transport and turbulence history is neglected in the mixing length hypothesis, unlike in point equilibrium, it cannot be applied to complex flows [26].

2.10. One-Equation Model

In order to associate the characteristic flow velocity with the root mean square of the turbulent kinetic energy, differential equations, rather than algebraic equations, were used to include the effects of turbulence diffusion and convection on the characteristic velocity. From this, one differential model equation was developed wherein the characteristic velocity is the turbulent kinetic energy, which is calculated via a differential equation. The turbulent flow velocity scale is used in combination with transport, diffusion, convection, and turbulence history in one-equation model. It is found that these transport phenomena are significant, and these models also have a distinct advantage over zero-equation models. One of the main reasons to study such models is that they are simple; however, such models are not suited to study highly complex flows [26].

2.11. Two-Equation Model

Complex flow conditions require precise assessment of transport and diffusion impacts from characteristic dimensions. The development of two-equation differential models of turbulent viscosity became necessary. All these models determine turbulent viscosity through the relation Vt=lk^0.5. The models develop a variable z=k^m L^n composed of m and n constants and use Navier-Stokes equations to derive Z exactly. The research study declines to use L as a variable because it approaches the problem by treating Z together with turbulent kinetic energy k and characteristic length as the unresolved aspect. The development of diverse two-equation models proceeds from different m and n values according to Table 1, found in [26].

Table 1. Various Two-Equation turbulence models

m	n	Z	Dimension	Model
0	1	L	M	k − L
1	1	KL	M^3/T	k − kL
2/3	–1	$K^3/2/L$	M^2/T^3	k − ε
1	–2	k/L^2	$1/T^2$	k − w
1/3	–1	K1/3/L	1/T	k − f

All models, in practice, yield equivalent results that can be arranged in a single mathematical expression. The standard $k-\varepsilon$ model represents the most popular choice from two-equation models for turbulent flow analysis, according to reports [26].

2.12. The Standard $k-\varepsilon$ Model

The model considers $z=\frac{k^{\frac{2}{3}}}{l}$ and designates it as ε to denote the turbulent energy dissipation rate [26].

$$\varepsilon = \nu\overline{\frac{\partial u_1'}{\partial x_J}\frac{\partial u_1'}{\partial x_J}}. \tag{15}$$

Through Navier–Stokes equations, the transport equations for k and ε quantities appear as (16) and (17):

$$\frac{\partial k}{\partial t}+\bar{u}_i\frac{\partial k}{\partial x_i}=\frac{\partial}{\partial x_i}\left[\left(\nu+\frac{\nu_t}{\partial k}\right)\frac{\partial k}{\partial x_i}\right]+p-\varepsilon; \tag{16}$$

$$\frac{\partial \varepsilon}{\partial t}+\bar{u}_i\frac{\partial \varepsilon}{\partial x_i}=\frac{\partial}{\partial x_i}\left[\left(\nu+\frac{\nu_t}{\partial \varepsilon}\right)\frac{\partial \varepsilon}{\partial x_i}\right]+c_{1\varepsilon}\frac{\varepsilon}{k}p-c_{2\varepsilon}\frac{\varepsilon^2}{k}; \tag{17}$$

$$\nu_t=c_\mu\frac{k^2}{\varepsilon}; \tag{18}$$

$$p=\nu_t g=\nu_t\left[\frac{\partial\overline{u_t}}{\partial x_j}+\frac{\partial\overline{u_j}}{\partial x_i}\right]\frac{\partial\overline{u_t}}{\partial x_j}. \tag{19}$$

In the $k-\varepsilon$ model, the production and dissipation of turbulent kinetic energy are consistently assumed proportional to each other, such that the transport equations for k and ε quantities presume their production and dissipation are proportional. The standard $k-\varepsilon$ model is applicable for fully turbulent regions of a flow field; however, near walls, the local Reynolds number is consistently small, such that molecular viscosity effects dominate flow turbulence, consequently preventing the use of the standard $k-\varepsilon$ model in these regions [26].

Two solutions exist to overcome this limitation [26]:

2.13. Implementation of the Wall Function Method

Utilization of modified forms of the standard $k-\varepsilon$ model that account for molecular viscosity effects near walls, known as low-Reynolds $k-\varepsilon$ models.

2.14. Multi-Equation Models

Reynolds Stress Model (RSM) and Algebraic Stress Model (ASM) represent significant examples of multi-equation models. RSM represents one of the most advanced classical turbulence models that effectively tackles multiple limitations of the k model when predicting complex strain fields and significant body force conditions. Multi-equation models offer both realistic physical turbulence process representation and successful performance for free-stream flow together with near-wall flow as well as two-dimensional internal flows [24].

2.15. Introduction to Computational Software (FLOW 3D)

Computational fluid dynamics features FLOW 3D as one of its important commercial software solutions. Flow Science in the United States develops and supports this software program as it serves multiple engineering fields such as mechanical and fluid dynamics, metallurgy and chemical engineering, environmental engineering, water engineering hydraulics, and marine applications. The distinct element of this software enables free-surface flow simulation that proves crucial for hydraulic and hydrodynamic engineering applications.

FLOW 3D's capabilities in hydraulic engineering include modeling cavitation phenomena, air entrainment and dispersion in fluid flow, wall stresses, porous media, sediment scour, shallow flows,

turbulent and laminar flows, and floating object movement. FLOW 3D offers five turbulence models: zero-equation, one-equation, two-equation ($k-\varepsilon$ and RNG), and Large Eddy Simulation.

FLOW 3D serves as an appropriate model for complex CFD problems with broad applications. The program is applicable to three-dimensional unsteady flows with free surfaces and complex geometries. FLOW 3D employs two numerical techniques for geometric simulation [27]:

- Volume of Fluid (VOF) method, applied to represent fluid behavior at free surfaces
- Fractional Area/Volume Obstacle Representation (FAVOR) method, utilized for simulating solid surfaces and volumes such as geometric boundaries [27]

The modeling utilized results from experiments conducted by Babak Navaee et al. (2016) on standard ogee spillways with flip buckets at 32 and 52° takeoff angles, as well as without buckets. In the laboratory model, energy dissipation in this type of spillway was examined through 21 experiments with flow rates ranging from 330 to 864 L/min. The physical laboratory spillway model was constructed according to USBR standards with the height of 27.2 cm, length of 40 cm, and width of 30 cm, including a rectangular block (height of 6.6 cm, length of 10 cm, and width of 30 cm) and two flip buckets (length of 10 cm, width of 30 cm, and radii of 12 and 19 cm) made of polyethylene using CNC machinery. The experiments were conducted by placing the rectangular block and buckets at the end of the ogee spillway [1].

The practical and laboratory phases of this research were conducted in the Hydraulics Laboratory of Maragheh University, Maragheh, Iran, using a flume with a length of 6 m, width of 0.3 m, and height of 0.45 m. Fig. 1 shows the laboratory flume cross-section (a) and ogee spillway (b), while Fig. 2 displays the flip buckets and rectangular blocks with their dimensions [1].

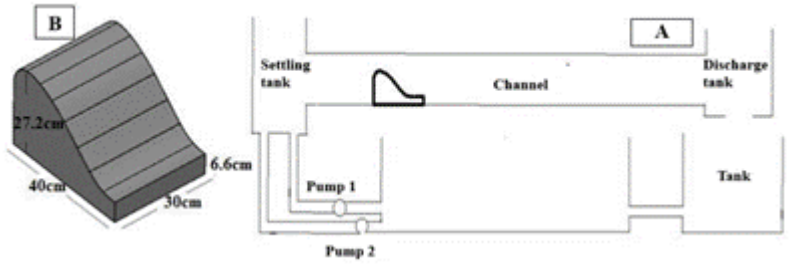

Figure 1. Laboratory flume cross-section (a) and ogee spillway (b).

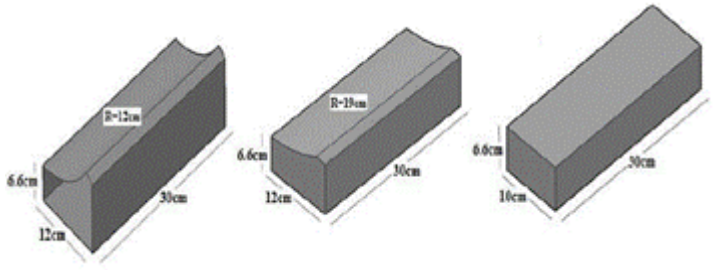

Figure 2. Flip buckets and rectangular block.

Flow rate was measured with 0.001 accuracy using two tachometers installed at the end of the pumps before entering the stilling basin [1].

Selection of Turbulence Model between k-ε and RNG in Modeling

For validation and selection of the turbulence model, numerical modeling was performed using FLOW 3D software with identical geometry hydraulic conditions but different turbulence models. The results comparing the maximum fluid throw length are shown in Table 2.

Table 2. Comparison of different turbulence models' results for fluid jump length with reference laboratory results

	RNG		**$k-\varepsilon$**		**Experimental results [15]**
Q (L/min)	Max L (cm)	Error (%)	Max L (cm)	Error (%)	Max L (cm)
508	20/2	5/2	20/4	6/25	19/2
597	26/6	5/97	26/8	6/77	25/1
659	33/1	6/78	33/3	7/4	31

The RNG turbulence model provides better accuracy with a reduced error percentage as compared to the $k-\varepsilon$ model. The RNG turbulence model became the selected choice for modeling purposes in this research. The largest error in jump length measurement took place at a flow rate of 659 L/min, with an error amounting to 6.8%.

3. Results and Discussion

3.1. Numerical Model Sensitivity to Meshing

Numerical modeling of projected flow requires meshing as an essential factor which can be implemented through different methods beyond geometry.

Multiple blocks can be created for meshing in FLOW 3D numerical software, defining each numerical model as single-block or multi-block. Each block can be specified with different dimensions and mesh numbers to achieve acceptable sensitivity and obtain various results. Higher mesh numbers and smaller sizes create appropriate sensitivity and acceptable results with lower errors in modeling. Several numerical modeling approaches were implemented:

- Single-block model with 5 mm mesh cells for 5 sec
- Set for analysis with 0.01-time steps, total computational cells amount to (total active cells 1,262,320)

  Additionally, the total number of cells (active and inactive) are 1,451,298, with total active cells at 1,262,320.

Active cells include:

- Real cells used for flow equation solving (1,185,330)
- Real open cells (1,181,212)
- Fully blocked real cells (4,118)
- External boundary cells (76,990)
- Inter-block boundary cells (0)

Fig. 3 below shows the single-block numerical model with specified 5 mm meshes.

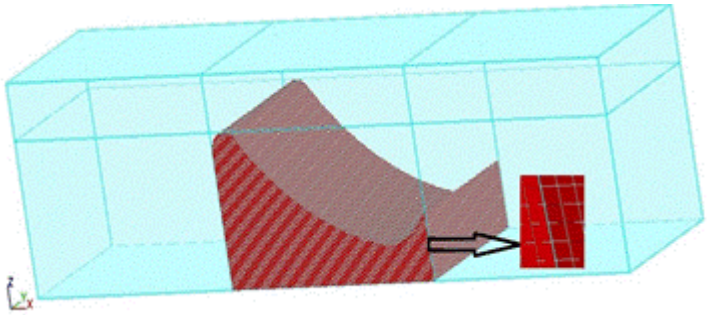

Figure 3. The numerical model meshes with one block.

The growth rate in the laboratory with a flow rate of 597 L/min is 0.715, whereas in the numerical model, the ΔEr value at different points around the projectile is mentioned in Table 3. In this Table, the sample numbers are designated such that sample (11) indicates the first point in zone zero, which is the area before the spillway, and sample (12) indicates the first point in zone one, which is the area after the spillway. For each zone, the x, y and z coordinates of the point of interest are specified in the Table.

Table 3. Hydraulic energy levels at points with 597 L/min flow rate and 5 mm mesh

Sample	X(m)	Y(m)	Z(m)	E(m)	ΔE_r = = $(E_0 - E_1) / E_0$	Error(%)
01	1.2157e+01	7.3610e+0	2.5378e-03	3.3194e-01	0.0759	6.15
11	1.3397e+01	7.3610e+0	2.5378e-03	0.79897e-02		
02	1.2072e+01	7.3611e+0	2.5379e-03	3.3189e-01	0.758	6
12	1.3412e+01	7.3660e+0	2.5379e-03	0.80140e-02		
03	1.2102e+01	7.3612e+0	2.5380e-03	0.33179e-01	0.726	1.4
13	1.3417e+01	7.3661e+0	2.5380e-03	9.0723e-02		

The ΔEr value obtained in the numerical model differs from the laboratory model, with an average error of 4.4% across these points, which is acceptable and suitable.

3.2. The Single-block Model with 5 mm and 4 mm Cells for 5 Sec

Five mm cells were used to create the front and back sections of the block because these areas lack a spillway while four millimeter cells were used for the middle section containing the spillway. This configuration allows the numerical model to operate as a single block through analysis of 5 sec with 0.01 time steps. There are 1,952,778 computational cells in relation to the active cells within the model.

The analysis shows that the study contains 2,314,622 cells which includes both active and inactive cells while the total active cells number reaches 1,952,778.

Active cells consist of:

- The total number of real cells that participated in flow equation calculations reached 1,850,578
- Real open cells (1,844,081)
- Completely blocked real cells (6,497)
- External boundary cells (102,200)
- Inter-block boundary cells (0)

The laboratory ΔEr at 597 L/min flow rate is compared with the numerical model, and the error rates at various points around the projectile are listed in Table 4.

Table 4. Hydraulic energy levels at points with 5 mm and 4 mm mesh in single-block configuration

Sample	X(m)	Y(m)	Z(m)	E(m)	$\Delta E_r = (E_0 - E_1) / E_0$	Error(%)
01	1.2057e+01	7.3635e+0	2.0012e-03	3.3195e-01	0.716	0.13
11	1.3374e+01	7.3635e+0	2.0012e-03	9.4099e-02		
02	1.2063e+01	7.3635e+0	2.0012e-03	3.3192e-01	0.710	0.069
12	1.3379e+01	7.3635e+0	2.0012e-03	9.5984e-02		
03	1.2069e+01	7.3635e+0	2.0012e-03	3.3190e-01	0.704	0.15
13	1.3385e+01	7.3635e+0	2.0012e-03	9.7984e-02		

The computed ΔEr shows acceptable deviation from the laboratory model to the extent of less than 0.7% due to denser mesh structure.

3.3. The Three-block Model with 5 mm and 4mm Cells for 5 Sec

A numerical model consisting of three blocks uses 5 mm cells for blocks one and three with no spillway and 4 mm cells for block two with the spillway and operates for 5 sec with a time step of 0.01. The computational system has 1,603,195 cells for numerical processing and also includes 1,603,195 active cells that demonstrate an adequate and appropriate level of responsiveness and maintain acceptable levels of error.

The analysis shows that the total quantity of cells reached 1,973,208, of which 1,603,195 cells were categorized as active.

Active cells consist of:

- The enumeration of real cells which executed flow equation calculations amounted to (1,479,328)
- Real open cells (1,472,831)
- Completely blocked real cells (6,497)
- External boundary cells (88,640)
- Inter-block boundary cells (35,227)

Fig. 4 below illustrates the numerical model meshes with three blocks.

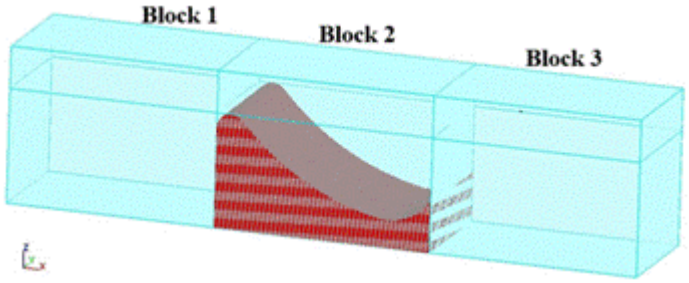

Figure 4. Numerical model meshes with three blocks.

The laboratory ΔEr value is 0.715 at a flow rate of 597 L/min, which has been compared with the numerical model at various points around the projectile, and the error rates are shown in Table 5.

Table 5. Hydraulic energy levels at points with 5 mm and 4 mm mesh in a three-block configuration

Sample	X(m)	Y(m)	Z(m)	E(m)	ΔE_r = = $(E_0 - E_1) / E_0$	Error(%)
01	1.2057e+01	7.3560e+0	0.24739e-03	3.3197e-01	0.705	1.4
11	1.3397e+01	7.3560e+0	0.24739e-03	0.97683e-02		
02	1.2062e+01	7.3560e+0	.24739e-03	3.3197e-01	0.721	0.084
12	1.3407e+01	7.3560e+0	7.4199e-03	0.92570e-02		

The measurements of ΔEr deviate from laboratory values at a 1.12% average discrepancy.

The numerical models in single-block and three-block configurations show acceptable error rates for both simulation types. The number of active cells used to solve flow equations decreased when the model evolved from a single-block to a three-block configuration. When assessing the results between single-block and three-block numerical models with their distinct ΔEr error rates, one can determine that complex geometries benefit from three-block modeling yet simple geometries benefit from more blocks, reducing the cell count but increasing the error margin. The single-block numerical model with two different mesh sizes of 4mm and 5mm demonstrates suitability for analytical purposes.

3.4. Impact of Froude Number at the Flip Bucket Edge on Maximum Jump Length and Height

According to this study, the Froude number at the flip bucket edge determines the greatest length of fluid jumps. Studies within the numerical model evaluated Fr = 3.9, 4.21, 4.45 using identical geometry to determine maximum jump length in centimeter as shown in Fig. 5.

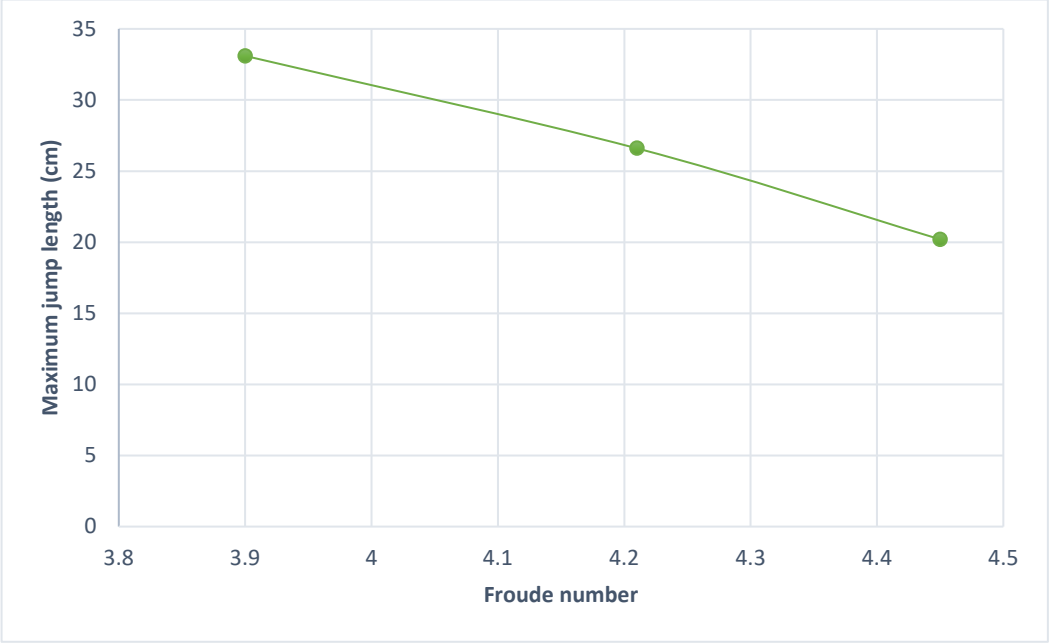

Figure 5. Changes in maximum jump length relative to Froude number at the flip bucket edge.

According to Fig. 5, it is clear that as the Froude number increases, the maximum jump length decreases, which aligns with the results of Navai et al. [28] and Mousavi Jahromi and Omidvarinia [14] experiments.

The analysis of Froude number at the flip bucket edge relative to maximum jump height was also conducted with different Froude numbers (Fr = 3.9, 4.21, 4.45), and the results are expressed in centimeters, shown in Fig. 6.

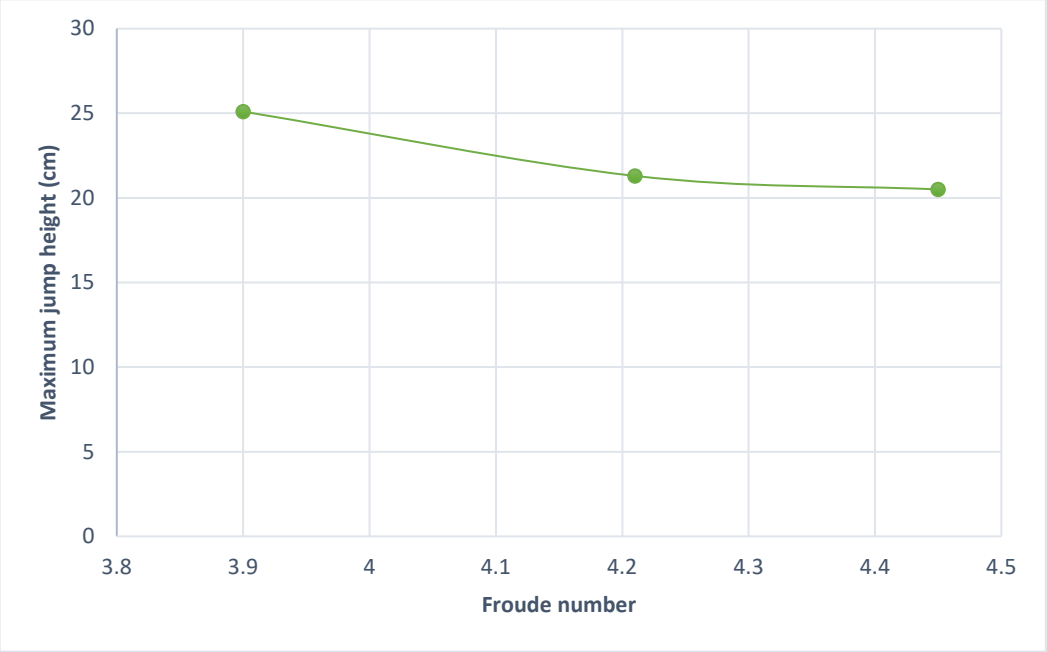

Figure 6. Changes in maximum jump height relative to Froude number at the flip bucket edge.

The results of Heller et al. [8] showed that jump height decreases with increasing Froude number, which is consistent with the modeling results shown in Fig. 6.

3.5. The Impact of Flow Rate on Maximum Jump Length and Height

The analysis of flow rate relative to maximum jump length was conducted with flow rates of 508, 597, and 659 L/min, and the results are expressed in centimeters, shown in Fig. 7.

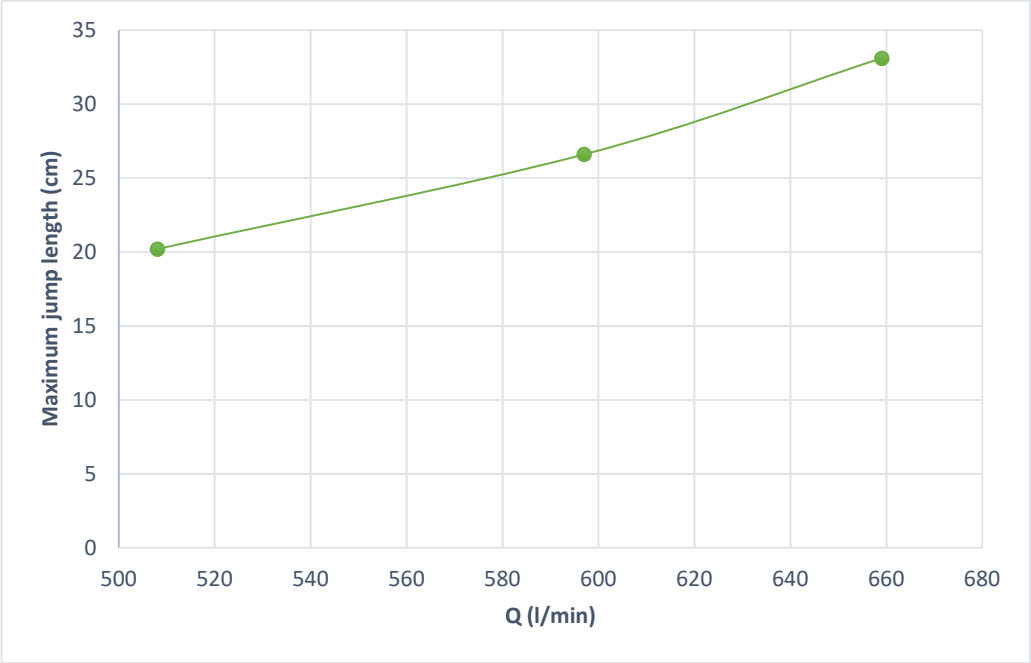

Figure 7. Changes in maximum jump length relative to flow rate.

According to the results and Fig. 7, with increasing flow rate, the maximum jump length increases, which aligns with the laboratory model results of Navai et al. [28].

The analysis of flow rate relative to maximum jump height was also conducted with flow rates of 508, 597, and 659 L/min, with results expressed in centimeters and shown in Fig. 8.

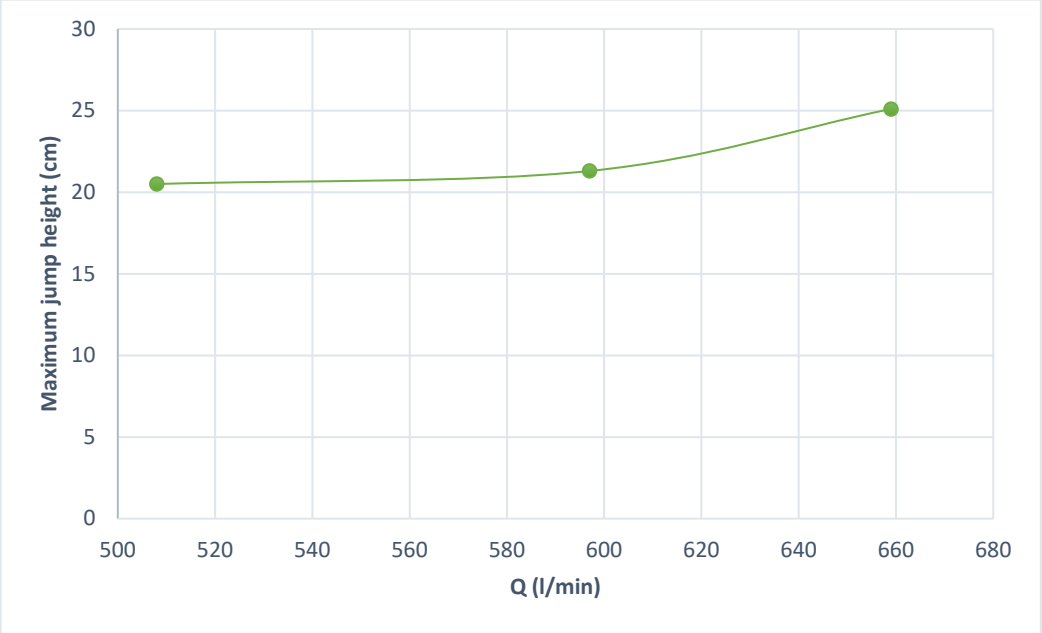

Figure 8. Changes in maximum jump height relative to flow rate.

Based on the results and Fig. 8, it is evident that with increasing flow rate, the maximum jump height increases, which aligns with the laboratory results of Mousavi Jahromi and Omidvarinia [14].

3.6. Impact of Flip Bucket Angle on Maximum Jump Length and Height

Numerical modeling of the bowl-shaped flip bucket generated maximum projectile length and maximum fluid projectile height results using an analysis flow rate of 508, 597, and 659 L/min under identical geometric conditions at a 52° angle with a 12 cm radius of curvature.

The same flow conditions (508, 597, and 659 L/min) were used for running the numerical model after changing the flip bucket geometry to a 32° angle with a 19 cm radius of curvature. Results were analyzed on this configuration.

Results from the numerical model appear in Table 6 following alterations to flip bucket angle and curvature.

Table 6. Maximum jump length, jump height, and Froude number for different flip bucket geometries

Turbulence Model RNG	**Projectile Angle: 52° Arc Radius: 19 cm**			**Projectile Angle: 32° Arc Radius: 12 cm**		
Q (L/min)	508	597	659	508	597	659
Max L (cm)	20.2	26.6	33.1	31.3	34.8	39.6
Fr	4.45	4.21	3.9	4.35	4.1	3.78
Max h (cm)	20.5	21.3	25.1	12.2	13.8	15.6

Based on Table 6 results, graphs of maximum jump length, maximum jump height, and Froude number with different launch angles relative to flow rate have been specified. Fig. 9 shows the maximum jump length relative to different flow rates of 508, 597, and 659 L/min.

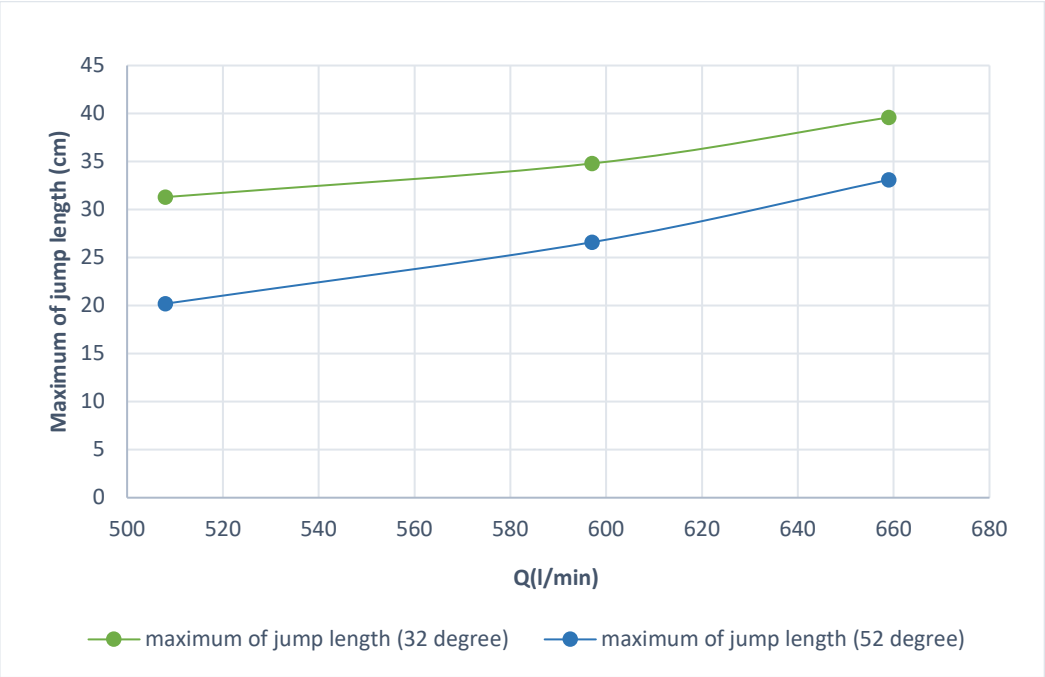

Figure 9. Changes in maximum jump length with jump angles of 52 and 32° relative to flow rate.

The results and Fig. 9 show that changing the flip bucket angle from 52 to 32° increases the maximum fluid jump length, which aligns with the laboratory results of Heller et al. [8].

Fig. 10 shows the maximum fluid jump height relative to different flow rates of 508, 597, and 659 L/min.

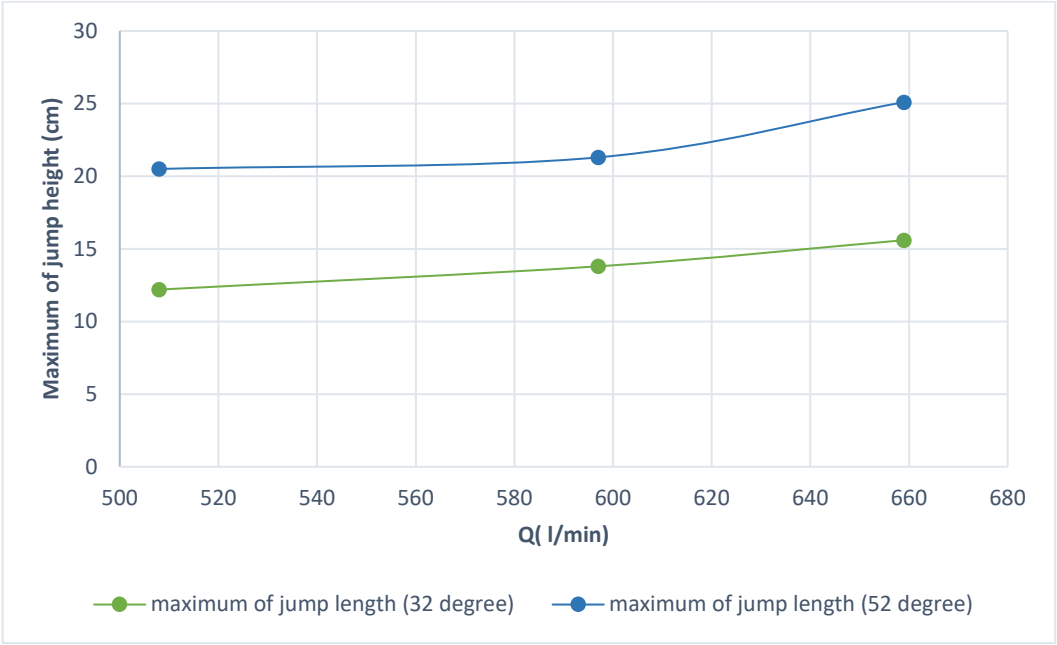

Figure 10. Changes in maximum jump height with jump angles of 52 and 32° relative to flow rate.

The results and Fig. 10 show that changing the flip bucket angle from 52 to 32° decreases the maximum fluid jump height, which aligns with the laboratory results of Mousavi Jahromi and Omidvarinia [14] and Navai et al. [28].

Fig. 11 shows the maximum Froude number at the flip bucket edge relative to different flow rates of 508, 597, and 659 L/min.

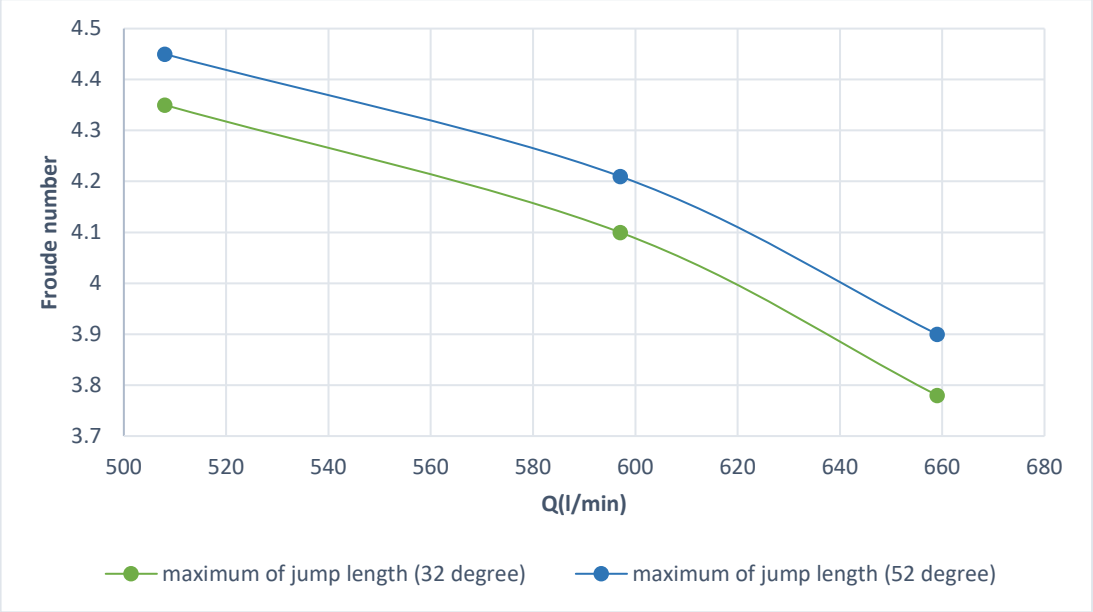

Figure 11. Changes in Froude number at the flip bucket edge with jump angles of 52 and 32° relative to flow rate.

Fig. 11 shows that changing the flip bucket angle from 52 to 32 degrees decreases the Froude number at the flip bucket edge, which aligns with Mousavi Jahromi's [14] results.

Energy Dissipation

Analysis of results shows that the energy loss ratio (output to input energy) decreases with increasing flow rate from 508 to 659 L/min, and changing the flip bucket angle from 52 to 32° reduces energy dissipation in the bowl-shaped flip bucket. Table 7 shows the energy loss relative to flow rate and flip bucket angle.

Table 7. Energy loss relative to flow rate and flip bucket angle

Flow Rate (L/min)	Energy Loss at 52° Projectile Angle	Energy Loss at 32° Projectile Angle
508	0.766	0.727
597	0.737	0.702
659	0.728	0.696

In Fig. 12, changes in energy loss relative to flow rate and projectile angle are shown.

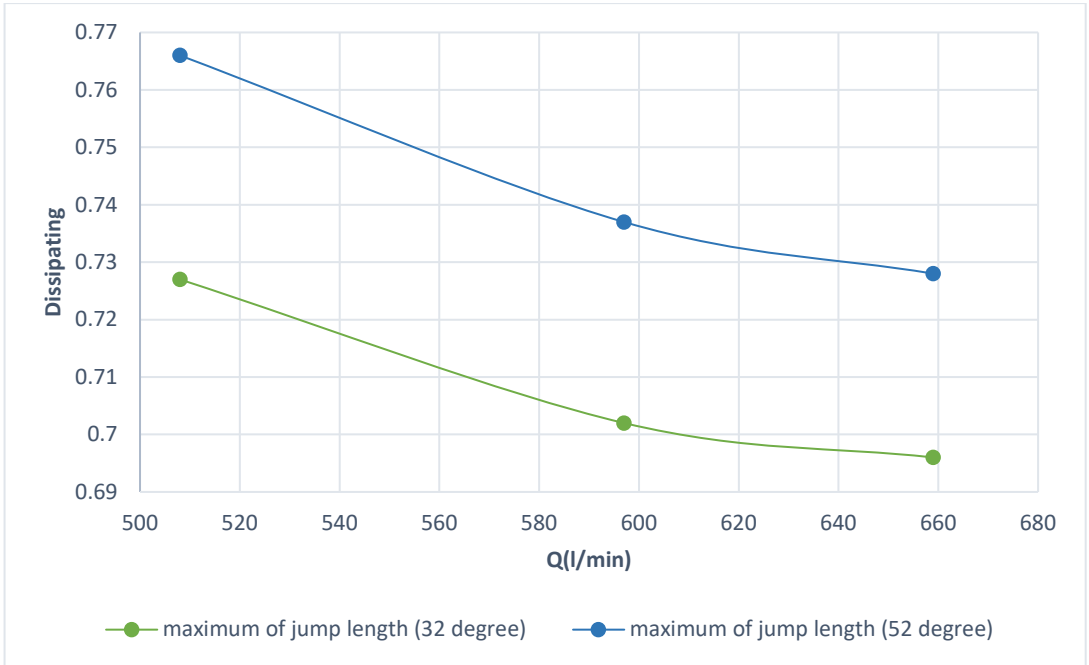

Figure 12. Changes in energy loss relative to flow rate and projectile angle.

Based on comparing the numbers in Fig. 12, the effect of angle changes on energy loss is greater than flow rate changes.

4. Conclusion

The procedure through which dams release energy stands among the critical matters regarding their design. Energy dissipation through dams requires the implementation of multiple systems that perform this function. Ski-jump spillways stand out as critical among these structures, while the exit jet of these structures experiences multiple difficulties, including jet diffusion and downstream erosion. More affordable evaluations of challenging topics become possible through the combination of developed software and hardware systems for numerical simulation. Using meshing and the FAVOR method for simulating the mesh generation process has made modeling complex geometries easier for users. In this research, square meshing with dimensions of 4 mm and 5 mm was used.

This research used CFD methods to investigate and numerically model the effects of various geometric and hydraulic parameters related to ski-jump spillways on the exit jet. The RNG turbulence model was used to examine parameters affecting the exit jet from the spillway, and numerical results were compared and validated with existing experimental studies and measurements. Changes related to maximum jump length and maximum jump height were also examined. The results obtained from this study are presented in this chapter.

The specific results of this research are as follows:

1. In this research, using FLOW 3D software and the RNG turbulence model, the effects of various geometric and hydraulic parameters related to ski-jump spillways on the exit jet were investigated. Given the alignment obtained between the software and experimental results, it can be stated that this software is suitable and highly capable of analyzing various issues related to energy dissipation, ski-jump spillways, and open channel flows. The RNG turbulence model results show better agreement with experimental results than the $(k-\varepsilon)$ turbulence model.

2. In this research, the relative error in energy reduction between experimental results and numerical model results was less than 5%, and the error related to maximum jump length was less than 7%.

3. In this research, the flow rate range was considered between 508 and 659 L/min. With increasing flow rate in a specific and fixed geometry, the maximum jump length and maximum jump height increased, and consequently, the Froude number decreased. The design process should account for the increased maximum length and height that occurs at lower Froude numbers. The reduction of the Froude number to achieve maximum height and maximum jump length becomes possible through increased flow rates. The acceptable flow rate increase needs to maintain a safe operating zone for spillway capacity during this process.

4. Changes in ski-jump spillway geometry were also investigated in this research. Geometric changes included varying the spillway angle from 52 to 32° and changing the arc radius from 12 cm to 19 cm. These geometric changes had a direct and significant impact on the maximum spillway length, maximum spillway height, and Froude number at the spillway lip.

5. Analysis of the numbers showed that with decreasing spillway angle, the maximum jump length increased while the maximum jump height decreased. The effect of angle change on reducing maximum jump height was more noticeable compared to the maximum jump length. With changes in spillway geometry and a reduction in spillway angle, the Froude number decreased, although this decrease was not significant. If the angle reduction becomes greater, this change in the Froude number will consequently increase as well.

References

1. Santorok, F. Hydraulics of Dams and Reservoirs. Noavar Publication, Tehran, 2012. Pp. 86–102.
2. Olsen, N., Kjellesvig, H.M. Three-dimensional numerical flow modeling for estimation of spillway capacity. Journal of Hydraulic Research, 1998, 36(5), pp. 775–784. DOI: 10.1080/00221689809498602
3. Meilan, Q.L., Fujisak, K., Tanaka, K. Sediment re-suspension by turbulent jet in an intake pond. Journal of Hydraulic Research, 2000, 38(5), pp. 323–330. DOI: 10.1080/00221680009498313
4. Savage, B., Johnson, M. Flow over ogee spillway: Physical and numerical model case study. Journal of Hydraulic Engineering, 2001, 127(8), pp. 640–649. DOI: 10.1061/(asce)0733-9429(2001)127:8(640)
5. Ho, H., Boyes, K., Donohoo, S., Cooper, B. Numerical flow analysis for spillways. Proceedings of 43rd ANCOLD Conference, Hobart, Tasmania, 2003, pp. 24–29.
6. Sarker, M.A., Rhodes, D.G. Physical modeling and CFD applied to hydraulic jumps. Cranfield University Report, Institute of Technology, Bangladesh, 2002. Pp 552–563.

7. Weilin, X., et al. Experimental investigation on the influence of aeration on plane jet scour. Journal of Hydraulic Engineering, 2004. 130(2), DOI: 10.1061/(asce)0733-9429(2004)130:2(160)
8. Heller, V. Ski Jump Hydraulics. Journal of Hydraulic Engineering, 2005. 131, pp. 347–355. DOI: 10.1061/(asce)0733-9429(2005)131:5(347)
9. Pagliara, S., Hager, W.H., Minor, H.-E. Hydraulics of plane plunge pool scour. Journal of Hydraulic Engineering, 2006, 132(5), DOI: 10.1061/(asce)0733-9429(2006)132:5(450)
10. Dargahi, B. Experimental study and 3D numerical simulations for a free-overflow spillway. Journal of Hydraulic Engineering, 2006, pp. 899–907. DOI: 10.1061/(asce)0733-9429(2006)132:9(899)
11. Steiner, R., Heller, V., Hager, W.H., Minor, H.-E. Deflector ski jump hydraulics. Journal of Hydraulic Engineering, 2008, 134, pp. 562–574. DOI: 10.1061/(asce)0733-9429(2008)134:5(562)
12. Kavianpour Esfahani, M.R., Ajdari Moghadam, M., Goodarzi, M. Experimental study of flow rate and tailwater depth effects on maximum scour depth downstream of ski jump spillways, Proceedings of 10th Hydraulic Conference, 2011. Pp. 128–136.
13. Arefpour, M., Fathi Moghadam, M., Douraghi, A., Hosseini, A., Tajaran, A. Investigation of hydrodynamic pressure distribution and instantaneous pressure fluctuations along the ski jump spillway of Balaroud Dam, Proceedings of 9th International Seminar on River Engineering, 2012. Pp. 246–255.
14. Mousavi Jahromi, S.H., Omidvarinia, M. Effect of threshold length and angle in triangular deflectors on overall exit jet trajectory, Water and Soil Resources Protection, 2012, 1(4), pp. 1–17.
15. Askari, M., Ghomeshi, M. Energy losses due to deflector in simple ski jump spillway and ski jump spillway with approaching channel, Journal of Water and Soil Knowledge, 2013. 23. Pp. 340–349.
16. Nikpour, M.R., Salmani Jelodar, Z., Hosseinzadeh Dalir, A., Sani Khani, H., Shoja, F. Application of finite element and finite volume methods in water flow analysis over ogee spillway (case study: Damghan Dam), Iranian Water Research Journal, 2014, 8(14), pp. 55–63.
17. Eshrati, T., Fazloli, R., Sanei, M., Emadi, A. Experimental investigation of hydraulic performance of ogee spillway and downstream channel in axial curve conditions, Journal of Water and Soil Knowledge, 2015. 29(4). Pp. 98–110.
18. Kakeshpour, M., Pirestani, M.R., Zakeri Niri, M. Investigation of ski jump deflector shape effect in chute spillway using numerical model, Journal of Water and Soil Knowledge, 2016, 23(5). Pp 841–857.
19. Fazlollahnejad, M., Hosseini, K., Karami, H., Farzin, S. Investigation of flow characteristics in Golvard Neka Dam chute spillway using computational fluid dynamics, Environment and Water Engineering, 2016. 3. Pp. 411–423.
20. Zhenweia, M., Zhiyan, Z., Tao, Z. Numerical simulation of 3D flow field of spillway based on VOF method, Proceedings of International Conference on Modern Hydraulic Engineering, 2012, 28. Pp. 808–812. DOI: 10.1016/j.proeng.2012.01.814
21. Sharif, N., Rostami Ravori, A. Experimental and numerical study of the effect of flow separation on dissipating energy in compound bucket, APCBEE Procedia, 2014, 9. Pp. 334–338. DOI: 10.1016/j.apcbee.2014.01.059
22. Fadaei-Kermani, E., Barani, G.A. Numerical simulation of flow over a spillway based on the CFD method, Scientia Iranica A, 2014, 21(1). Pp. 91–97.
23. Parsaie, A., Dehdar-behbahani, S., Hamzeh haghiabi, A. Numerical modeling of cavitation on spillway's flip bucket, Frontiers of Structural and Civil Engineering, 2016, 10(4). Pp. 438–444. DOI: 10.1007/s11709-016-0337-y
24. Barani, G.A., Yousef Abbasi, P. Energy dissipation in hydraulic structures (field study of energy dissipating structures), Amirkabir University of Technology, Jahad Daneshgahi Publications, 2009.
25. Pope, S.B. Turbulent Flows, Cambridge: Cambridge University Press, 2000, p. 771 DOI: 10.1017/cbo9780511840531
26. Flow Science, Flow-3D User Manual, [Online], URL: http://www.flow3d.com/ (reference date: 10.02.2026).
27. Goodarzi, M. Study of erosion downstream of ski jump spillways using CFD method. Master's Thesis, University of Sistan and Baluchestan, 2011.
28. Navaei, B., et al. Experimental study of the effect of ski jump bucket at the end of ogee spillway on energy dissipation and throw length, Journal of Water and Soil Knowledge, 2016, 26(3-2). Pp. 133–142.

Information about the authors:

***Saeid Mohammadalizadeh**,*
ORCID: https://orcid.org/0009-0000-7574-9313
E-mail: saeidmhmdalizadeh74@gmail.com

***Ali Yasaei**,*
E-mail: aliyasaei5@gmail.com

***Alireza Mardookhpour**,*
ORCID: https://orcid.org/0000-0001-8054-8209
E-mail: AR.mardookhpour@iau.ac.ir

Received 31.03.2025. Approved after reviewing 18.10.2025. Accepted 20.10.2025.